PREPRINT doi:10.1029/2021GL096789

Syntectonic sediment recycling controls eolian deposition in eastern Asia since ~8 Ma

Haijian Lu[1, 2, *], Marco G. Malusà[3], Zhiyong Zhang[4], Licheng Guo[4], Xuhua Shi[5], Jiacan Ye[1], Shengping Sang[1], Shangfa Xiong[4], Jiawei Pan[1, 2], Haibing Li[1, 2]

[1]Key Laboratory of Deep-Earth Dynamics, Institute of Geology, Chinese Academy of Geological Sciences, Baiwanzhuang Road #26, Beijing 100037, China.

[2]Southern Marine Science and Engineering Guangdong Laboratory, Guangzhou 511458, China.

[3]University of Milano-Bicocca, Piazza della Scienza 4, 20126 Milano, Italy.

[4]Institute of Geology and Geophysics, Chinese Academy of Sciences, Beijing 100029, China.

[5]School of Earth Sciences, Zhejiang University, Hangzhou 310027, China.

Corresponding author: Haijian Lu (email: haijianlu2007@126.com)

Key points:

- A sediment recycling event starting at ~8 Ma is confirmed by new magnetostratigraphic and detrital apatite fission-track data.
- A new syntectonic sediment recycling model is proposed to explain the origin of eolian deposition in eastern Asia.
- A connection between sediment recycling and eolian deposition is supported by multi-proxy datasets of fluvio-lacustrine deposits.

Abstract

Global cooling and/or Tibetan Plateau uplift have long been regarded as the principal drivers of late Cenozoic central Asian aridification and the resulting widespread accumulation of eolian deposits in eastern Asia. However, these two factors are unable to form large source areas of fine-grained sediments enhancing eolian deposition synchronously from northern Tibet to North Pacific. Here we provide magnetostratigraphic and detrital apatite fission-track evidence for a major sediment recycling event in northern Tibet at ~8 Ma, coeval with a sudden increase in eolian deposition, which we ascribe to syntectonic erosion of uplifted friable fluvio-lacustrine sediments and selective entrainment by the westerly winds during basin deformation. Our results emphasize the importance of widespread and persistent occurrence of fine-grained sediments along the pathway of westerlies to produce voluminous dust deposits. These findings suggest that the onset of eolian deposition may not be directly related to global cooling or uplift of mountain ranges.

Plain Language Summary

A proper analysis of tectonic events and sedimentological processes is key to understanding the controlling factors of enhanced eolian deposition documented synchronously from northern Tibet to the North Pacific since ~8 Ma. In addition to the hypothesized sizable inland deserts, potential dust sources have been considered to be piedmont fluvial sediments and dry lake sediments in northern Tibet and central Asia. However, almost all these suggestions fail to explain the rapid expansion of eolian deposition in the Chinese Loess Plateau, which required a substantial increase

in the availability of fine-grained silts and clays in the source areas.

Here we confirm a major sediment recycling event favored by basin deformation in northern Tibet through an integrated analysis of magnetostratigraphy and detrital apatite fission tracks. This event led to the uplift of a large amount of friable fluvio-lacustrine sediments along the fold-thrust belts of northern Tibet, which coincided with this sudden increase of eolian deposition at ~8 Ma. We suggest a causal link, favored by the action of the westerly winds, between uplift of basin strata in northern Tibet, sediment recycling and the substantial expansion of eolian deposition in eastern Asia, which gains support from multi-proxy analyses of fluvio-lacustrine sedimentary successions.

1 Introduction

The origin of arid environments in central Asia remains highly debated, with dominant causal factors suggested to be Cenozoic cooling (Lu et al., 2010), Tibetan Plateau uplift (Rea et al., 1998), or the retreat of the Paratethys Sea (Ramstein et al., 1997). Eolian deposits, as direct evidence for inland Asian aridification, are widely distributed in northern Tibet (Li et al., 2018; Licht et al., 2016), the Chinese Loess Plateau (CLP) (Guo et al., 2002; Liu, 1985; Qiang et al., 2011), the marginal seas of East Asia (Shen et al., 2017; Wan et al., 2007), and even the North Pacific (Rea et al., 1998). The major eolian deposits show a notable three-stage increase in spatial extent and accumulation rate, as exemplified by three loess and red clay sequences in the CLP, with depositional onset ages at 25-22 Ma (Guo et al., 2002; Qiang et al., 2011),

~8 Ma (Ding et al., 2001; Sun, 1998), and ~2.6 Ma (Liu, 1985). However, Earth's climate has undergone progressive long-term cooling since the latest Oligocene (Zachos et al., 2008), and the Himalaya-Tibetan orogen has experienced a prolonged uplift history since the collision of India with southern Eurasia at 60-50 Ma (Tapponnier et al., 2001; Yin, 2010). Northern Tibet, in close proximity to the CLP, has undergone substantial surface uplift since ~15 Ma (Molnar et al., 2010), at a time when no comparable expansion of eolian deposits is evident. Therefore, there is no clear correlation between the evolution of eolian deposition and global cooling or Tibetan Plateau uplift. This implies that the dynamics of loess accumulation in eastern Asia are not well understood yet.

Recent research has increasingly emphasized the importance of determining the source areas of these eolian deposits. In addition to the sizable inland deserts (Guo et al., 2002; Liu, 1985), potential dust sources have been considered to be piedmont fluvial sediments (Nie et al., 2014, 2018; Sun, 2002), and dry lake sediments in northern Tibet and central Asia (Kapp et al., 2011; Pullen et al., 2011). However, these would fail to explain the rapid expansion of eolian deposition in the CLP, which requires a substantial increase in the availability of silts and clays in the source areas.

In order to shed light on this issue, we performed a new magnetostratigraphic study of the ~6 km thick sedimentary succession of the Qaidam Basin (QB), the biggest intermontane basin in Tibet (Dahonggou section in Fig. 1), coupled with detrital apatite fission-track (AFT) analyses in two different sections exposed along the northern margin of the QB (Dahonggou and Lulehe sections in Fig. 1). The aim of our analyses is to better define the timing and regional extent of a Late Miocene sediment recycling event proposed by recent work (Pang et al., 2019; Wang et al., 2017), and to assess its relationships with tectonic deformation in northern Tibet and eolian deposition in eastern Asia. When critically discussed within the framework of available tectonic and stratigraphic data, our results allow us to propose a genetic linkage between syntectonic recycling of uplifted Miocene sediments in northern Tibet and the rapid expansion of eolian deposition documented in eastern Asia since ~8 Ma, providing new insights on the impact of global climate, regional tectonics, and central Asian aridification on the formation of the largest loess deposits worldwide.

2 Materials and Methods

A nearly continuous 5300-m composite stratigraphic section was sampled for magnetic measurements. It is composed of the western Dahonggou section, spanning from the lower part of the Ganchaigou Fm to the lower part of the Shizigou Fm, and the eastern Dahonggou section mainly including the Lulehe Fm (Fig. 1). We collected a total of 2244 samples from the same section studied by Wang et al. (2017), but with a 2.3 times higher sampling density. We also collected medium- to coarse-grained sandstone samples for detrital apatite fission-track analysis, including 8 samples from the 9-7 Ma stratigraphic interval of the Dahonggou section, and 11 samples from the ~5-km-thick Lulehe section (Fig. 1, S5). Details on the analytical methods employed for magnetic and fission-track analysis can be found in the Supplementary Information (Fig. S2-S5).

3 Results

3.1 Stratigraphic age model

A total of 1717, out of 2244 samples, yielded stable ChRM directions (Supplementary Dataset 1). The mean normal and reversal polarity directions of the 1717 samples are D=357.7°, I=39.8°, κ=12.3, α95=1.4 and D=184.3°, I=-35.6°, κ=10.9, α95=1.6 after tilt correction, respectively. The overall mean direction is D =3.7°, I =-29.1°, κ=10.5, α95 =1.1 before tilt adjustment and D =1.0°, I =37.8°, κ=11.4, α95 =1.1 after tilt adjustment. However, application of the reversal test for all the 1717 samples is negative, with gamma (6.69) being larger than gamma-critical (2.14) (McFadden and McElhinny, 1990). In order to pass the reversal test, we divide 1419 component directions clustering within 40° of the mean into 14 intervals (each one comprising 91-104 samples) (Table S1; Fig. S6). These grouped data pass a Class A reversal test, with gamma (2.53) being less than gamma-critical (3.98) (McFadden and McElhinny, 1990). The positive reversal test indicates that the magnetic remanence is most likely primary, though the monoclinal structure of the Dahonggou section (Fig. S1) precludes the application of a fold test. In total, 44 pairs of normal and reversed polarity intervals are identified (Fig. 2).

The age of the QB basal strata has long been debated and either referred to 52 Ma (Ji et al., 2017) or 25.5-21 Ma (Wang et al., 2017; Nie et al., 2020). Our new magnetostratigraphic data for the ~5300-m-thick Dahonggou section of the QB confirm the magnetozone sequence of Wang et al. (2017). In the correlation of the observed polarity zones to the Geomagnetic Polarity Time Scale (Hilgen, 2012), we emphasize the importance of the Mid-Miocene mammalian fossils discovered in the upper Ganchaigou Formation (Fm.) of the Dahonggou section (Li and Wang, 2015) as a reliable tie point. The results indicate that the deposits span the time interval of ~24-4.8 Ma (Fig. 2).

3.2 Magnetic susceptibility and grain-size data

Bulk magnetic susceptibility (MS) values range from 19.7 to 752.2 μSI, with an average of 220 μSI (Fig. 2; Supplementary Dataset 2). MS values gradually increase from ~24 to 10.8 Ma. They remain rather constant between 10.8 and ~8 Ma, and finally show a rapid decrease starting from ~8 Ma, with relatively low values since then (128 μSI on average). In a similar fashion, grain-size data show a sharp decrease in the finest (<63 μm) sediment fraction starting from ~8 Ma (Fig. 2 and Supplementary Dataset 3).

3.3 Detrital AFT data

A recent detrital AFT study of the Dahonggou section (Wang et al. 2017, Fig. 3A) revealed a Late Miocene age-trend reversal that was interpreted as the evidence for exhumation and erosional recycling of basin sediments into younger strata caused by thrusting and basin segmentation. A similar age-trend reversal was identified by Pang et al. (2019) in the Huaitoutala section at 9-7 Ma (Fig. 3B). The eight detrital AFT samples we have analyzed along the Dahonggou section in the 9 to 7 Ma stratigraphic interval not only provide additional compelling evidence for a major sediment recycling event in the Late Miocene in the QB, but conclusively restrict its age to 8 Ma. Our results are summarized in Fig. 3C. Grain-age distributions are polymodal, which provides evidence of a mixed provenance (e.g., Malusà and Fitzgerald, 2020), and include 112 to 123 single-grain ages ranging from 22.6 to 626 Ma. They were deconvolved into best-fit grain-age populations by BinomFit (Brandon, 2002) based on the automatic mode for searching and identifying the optimal number of significant peaks (Table S2-3; Fig. S7-8). All the analyzed samples yielded peak ages that are significantly older than the corresponding depositional age, which ensures that they reflect the thermochronologic age structure of the eroded bedrock. Different color intensities in the diagram of Fig. 3C indicate the different size of each grain-age population. Notably, in the 9 to 8 Ma stratigraphic interval, the age of all the populations systematically decreases moving upsection, as normally expected for the progressive unroofing of the eroding sources (Malusà and Fitzgerald, 2020). However, starting from 8 Ma, peak ages start increasing upsection, almost mirroring the age and size of the peaks characterizing the underlying strata deposited at 9-8 Ma, as expected in case of temporary storage and recycling of sediment previously deposited in the QB.

Similar results are provided by our detrital AFT data set from the Lulehe section (Fig. 3D), in the western portion of the northern QB (Fig. 1, S1), where the 11 sandstone samples yielded single grain-ages in the range of 16.4 to 684 Ma after dating 83 to 113 grains per sample. Magnetostratigraphic data for the Lulehe section are not available yet, and we thus performed a comparison with the Dahonggou section, exposed ~80 km apart, based on lithology, sediment thickness and sedimentological features (Zhuang et al., 2011; Fig. 1, S1). Also in this case, the stratigraphic interval likely corresponding to a depositional age of ~8 Ma displays a remarkable AFT age-trend reversal for all the grain-age populations detected by BinomFit, which confirms the regional extent of the sediment recycling event first detected in the Dahonggou section.

4 Discussion

Our results shed light on the relations between tectonic and sedimentary process in the study area. They are particularly relevant when discussed within the framework of existing studies on the tectonic evolution of northern Tibet and available time constraints on loess deposits in eastern Asia.

4.1 Evidence for basinward deformation onset at ~8 Ma in northern Tibet

A number of previous studies have suggested a marked thrust front-propagation and rapid uplift of Cenozoic sedimentary successions along the northern and southern margins of the QB (e.g., Wei et al., 2016; Fig. 4), taking place in the ~8 to 4.8 Ma (Wang et al., 2017) or even <2 Ma (Pang et al., 2019) time interval. A similar event is recorded in the smaller Linxia basin, northeastern Tibet (Zheng et al., 2003). Syntectonic growth strata are described in the Kumkol (Lu et al., 2018), Gonghe (Craddock et al., 2011), and Guide basins (Fang et al., 2005) (Fig. 4). Deformation likely led to sedimentary rocks exposure above the level of lakes previously located in the QB.

4.2 Rapid expansion of eolian deposits in eastern Asia at ~8 Ma

A marked expansion of wind-blown deposition occurred at widely separated places from northeastern Tibet to the North Pacific around 8 Ma (Figs. 4, 5). The most striking example is the initial accumulation of red clay deposits in the eastern part of the CLP at ~8 Ma (Ao et al., 2016; Ding et al., 2001; Qiang et al., 2001; Song et al., 2001; Sun, 1998; Fig. 4). The concurrent basal ages and extensive distribution of the red clay deposits indicate an abrupt increase in dust supply from the source areas. A period of high dust accumulation rate is observed in the western part of the CLP at 8-7 Ma (Guo et al., 2002; Fig. 5E). A major provenance shift in the CLP at 9.5-7 Ma is also suggested by analysis of the crystallinity index of fine-grained quartz grains (Ma et al., 2015; Fig. 5H). $^{87}Sr/^{86}Sr$ ratios and clay mineralogy of fluvial-lacustrine sequences in the Linxia and Xining basins also reveal an increase in eolian dust input at ~8 Ma, suggesting intensified eolian activity in northern Tibet at that time (Yang et al., 2019; Yang et al., 2017; Fig. 5F, G). Farther to the east, clay mineral assemblages of the silicate fraction of sediments from the southern Japan Sea indicate a rapid increase in eolian input from central Asia at ~8 Ma that was transported by the high-altitude westerly circulation (Shen et al., 2017; Fig. 5C). Additionally, a pronounced increase in mass accumulation rate of eolian dust transported by the East Asian winter monsoon was detected at ~8 Ma in the northern South China Sea (Wan et al., 2007; Fig. 5D), as well as in the central North Pacific where mass accumulation rates of eolian dust show a four-fold increase at that time (Rea et al., 1998; Fig. 5B).

4.3 Source-to-sink dynamics and the role of the mid-latitude westerly winds

Syntectonic uplift of fluvio-lacustrine sediments and their exposure to wind deflation in northern Tibet seem to have occurred concurrently with the rapid expansion of eolian deposition in eastern Asia around 8 Ma. Some studies have indicated the persistent occurrence of the westerly winds blowing across the QB and along the northern margin of the Tibetan Plateau since at least 42 Ma (Caves et al., 2015; Licht et al., 2016). Low-level winds can entrain and carry dust which is deposited downwind in the fluvial-lake systems of the Linxia and Xining basins in northeastern Tibet, forming pure eolian sequences on relatively flat and stable topography. Jet stream flows over Japan Sea and the North Pacific. This suggests a connection between the orogen-basin systems of northern Tibet and the downwind eolian deposits of East Asia by the mid-latitude westerly winds (Fig. 4).

In addition to the striking coincidence in timing, three lines of evidence can be used to support this linkage:

1) detrital zircon age spectra are very similar in the Cenozoic sediments of the QB and in the late Miocene-Pliocene loess-red clay sequences of the CLP (Bush et al., 2016; Gong et al., 2016; Nie et al., 2018; Wang et al., 2017; Fig. S9), both showing two major populations at 300–200 Ma and 500–400 Ma beside three minor age populations at 1.0–0.7 Ga, 2.0-1.5 Ga and 2.7–2.2 Ga.

2) the percentage of the 0-63 μm grain-size fraction that can be transported in

suspension by wind (Pye, 1987) shows a sharp decrease from > 80% to ~40 % in the Dahonggou section between ~8 and 7.2 Ma (Fig. 2). In combination with the sediment recycling event discussed above, it is possible that many fine-grained clastic particles were removed during sediment recycling in the northern Tibet fold-thrust belts by the the westerly winds to be deposited farther east, where a coeval sharp increase in mean grain size is observed, for example in the Zhuanglang section (Sun et al., 2015; Fig. 4B).

3) Magnetic susceptibility values also decrease rapidly in the Dahonggou section since ~8 Ma (Figs. 2 and 4), despite the observation that synorogenic coarse-grained sediments that are primarily derived from metamorphic and magmatic rocks are generally associated with high magnetic susceptibility values (Lu et al., 2014; Sun et al., 2005; Fig. S10). Such abrupt decrease can be explained by a selective removal of the finest (<63 μm) particles from the recycled coarse-grained strata since ~8 Ma, as these particles are usually enriched in magnetic minerals (e.g., Malusà and Garzanti, 2019). Entrainment of <63 μm magnetic grains by the westerly winds, and their deposition farther east, might also explain the dramatic increase in magnetic susceptibility values observed in the Qin'an section (Guo et al., 2002; Fig. 4B). Moreover, the low magnetic susceptibility of Qin'an sediments before 8 Ma provides further support to the proposed linkage between syntectonic sediment recycling and the entrainment of fine-grained particles by the westerly winds, because the sediment source providing dust after 8 Ma was not available before 8 Ma, until the uplift of the sedimentary successions at the margin of the QB.

5 Conclusions

The Miocene unconsolidated fluvio-lacustrine sediments exposed along the basin margin in northern Tibet were likely the largest source of airborne dust on Earth at ~8 Ma. Sediment recycling events revealed by detrital AFT dating of the QB strata indicate that at least 1500 m of dominantly fine-grained lacustrine sediments were exposed continuously above lake level along the northern margin of the QB since ~8 Ma, although their spatial extent is difficult to determine precisely. A total of ~1500-m-thick sediments in the northern QB may have acted as a sustained source of material for wind erosion and dust generation. However, the potential source area is not limited to the QB. Uplifted friable sediments along the margins of the Tarim, Junggar, and Hexi Corridor basins, as well as other sub-basins in northern Tibet, may have also contributed dust materials now preserved between northern Tibet and the North Pacific.

An important implication of our basin deformation-driven hypothesis is that the well-known eolian deposits in Asia may not be simply related to changes in plateau topography or global climate as previously suggested. Our results point instead to a major potential role of basin deformation and sediment recycling in controlling the onset and evolution of eolian deposition from northern Tibet to the North Pacific.

Open Research

Supplementary data supporting the conclusions is available on the Research Data Repository of the Figshare (https://doi.org/10.6084/m9.figshare.18093839). The data on which this article is based are also available in Bush et al. (2016), Gong et al. (2016), Lu et al. (2014), Nie et al. (2018), Pang et al. (2019), Sun et al. (2005) and Wang et al. (2017).

Acknowledgements

This study was supported by the Second Tibetan Plateau Scientific Expedition and Research Program (2019QZKK0901), the Key Special Project for Introduced Talents Team of Southern Marine Science and Engineering Guangdong Laboratory (Guangzhou) (GML2019ZD0201) and the China Geological Survey (DD20190059). We are most grateful to Zhiming Sun, Yong Cao and Aijun Sun with paleomagnetic measurement, to Hanchao Jiang and Hongyan Xu with grain size analyses, and to Kun Yun with figure preparation.

Figure captions

Fig. 1. Location maps of the study area and sampling sites. A: Digital elevation model (DEM) of the QB and surrounding orogenic belts. B: Geological map of the Dahonggou section, showing the distribution of different sampling sections (Ji et al., 2017; Wang et al., 2017; This study).

Fig. 2. Magnetic polarity stratigraphy of the Dahonggou section and its correlation to the geomagnetic polarity time scale (GPTS; Hilgen, 2012) and the polarity zone sequences of Wang et al (2017). Also shown are lithostratigraphy, the percentage of the <63 μm fraction of sediment grain size, magnetic susceptibility, declinations,

inclinations, and virtual geomagnetic pole (VGP) latitudes. The blue lines show 5-point average and the broken red lines represent general evolution trend.

Fig. 3. Detrital AFT data of the Dahonggou (A, C; Wang et al., 2017; this study), Huaitoutala (B; Pang et al., 2019), and Lulehe (D; this study) sections in the QB, and a schematic illustration of sediment recycling within the northern QB (E, F). Red, green and gray continuous curves indicate age trends (not best-fit lines) referred to progressive source-rock exhumation, whereas dashed curves indicate age trends referred to sediment recycling.

Fig. 4. Sketch diagrams showing a source-sink relationship between uplifted strata and downwind eolian deposits linked by the westerly winds. A: Relief map of West China. The hypothetical areal extent of elevated strata in the QB is based on the balanced cross-section restorations of Wei et al (2016). B: Block diagram demonstrating an integrated relationship among tectonic uplift, dust entrainment, and sediment recycling in the northern QB at ~8 Ma. The lower-right inset shows the evolution trends of lithology, the percentage of 0-63 μm grain size, magnetic susceptibility and the youngest detrital AFT population peak ages (P1) of the Dahonggou section between 11 and 5 Ma. The upper-right inset indicates the mean grain size data of the Zhuanglang sction between 10 and 6 Ma (Sun et al., 2015) and the magnetic susceptibility data of the uppermost 100 m of the Qin'an section (Guo et al., 2002).

Fig. 5. Time series of multi-proxy records showing increased eolian dust input at ~8 Ma. The stacked global deep-sea oxygen isotope record (A; Zachos et al., 2008) is

shown for comparison. The sites are in the North Pacific (B; Rea et al., 1998), Japan Sea (C; Shen et al., 2017), South China Sea (D; Wan et al., 2007), Chinese Loess Plateau (E, H; Guo et al., 2002; Ma et al., 2015), and northeastern Tibet (F, G; Yang et al., 2019; Yang et al., 2017).

References:

Ao, H., A. P. Roberts, M. J. Dekkers, X. Liu, E. J. Rohling, Z. Shi, Z. An, and X. Zhao (2016), Late Miocene–Pliocene Asian monsoon intensification linked to Antarctic ice-sheet growth, Earth and Planetary Science Letters, 444, 75-87.

Brandon, M. (2002), Decomposition of mixed grain age distributions using Binomfit., On Track, 24, 13-18.

Bush, M. A., J. E. Saylor, B. K. Horton, and J. Nie (2016), Growth of the Qaidam Basin during Cenozoic exhumation in the northern Tibetan Plateau: Inferences from depositional patterns and multiproxy detrital provenance signatures, Lithosphere, 8(1), 58-82.

Caves, J. K., M. J. Winnick, S. A. Graham, D. J. Sjostrom, A. Mulch, and C. P. Chamberlain (2015), Role of the westerlies in Central Asia climate over the Cenozoic, Earth and Planetary Science Letters, 428, 33-43.

Cogné, J. P. (2003), PaleoMac: a Macintosh application for reconstructions, Geochemistry Geophysics Geosystems, 4(1).

Craddock, W., E. Kirby, and H. Zhang (2011), Late Miocene–Pliocene range growth in the interior of the northeastern Tibetan Plateau, Lithosphere, 3(6), 420-438.

Ding, Z., S. Yang, S. Hou, X. Wang, Z. Chen, and T. Liu (2001), Magnetostratigraphy and sedimentology of the Jingchuan red clay section and correlation of the Tertiary eolian red clay sediments of the Chinese Loess Plateau, Journal of Geophysical Research: Solid Earth, 106(B4), 6399-6407.

Donelick, R. A., P. B. O'Sullivan, and R. A. Ketcham (2005), Apatite Fission-Track Analysis. Reviews in Mineralogy & Geochemistry.

Enkin, R. J. (1994), A computer program package for analysis and presentation of paleomagnetic data, Pacific Geoscience Centre, Geological Survey of Canada, 16, 16.

Fang, X., M. Yan, R. Van der Voo, D. K. Rea, C. Song, J. M. Parés, J. Gao, J. Nie, and S. Dai (2005), Late Cenozoic deformation and uplift of the NE Tibetan Plateau: Evidence from high-resolution magnetostratigraphy of the Guide Basin, Qinghai Province, China, GSA Bulletin, 117(9-10), 1208-1225.

Fisher, R. (1953), Dispersion on a sphere, Proceedings of the Royal Society of London. Series A. Mathematical and Physical Sciences, 217(1130), 295-305.

Gleadow, A. J. W., S. J. Gleadow, D. X. Belton, B. P. Kohn, M. S. Krochmal, and R. W. Brown (2009), Coincidence mapping-a key strategy for the automatic counting of fission tracks in natural minerals, Geological Society London Special Publications, 324(1), 25-36.

Gong, H., J. Nie, Z. Wang, W. Peng, R. Zhang, and Y. J. S. r. Zhang (2016), A comparison of zircon U-Pb age results of the Red Clay sequence on the central Chinese Loess Plateau, Scientific Report, 6(1), 1-6.

Guo, Z., W. F. Ruddiman, Q. Hao, H. Wu, Y. Qiao, R. X. Zhu, S. Peng, J. Wei, B. Yuan, and T. Liu (2002), Onset of Asian desertification by 22 Myr ago inferred from loess deposits in China, Nature, 416(6877), 159-163.

Hasebe, N., J. Barbarand, K. Jarvis, A. Carter, and A. Hurford (2004), Apatite fission-track chronometry using laser ablation ICP-MS, Chemical Geology, 207(3-4), 135-145.

Hilgen, F., J., Lourens, L. J., Van Dam, J. A. (2012), The Neogene period in Geologic Time Scale 2012 Vol. 2 (ed Gradstein, F. M. et al.) Ch. 29 923-978 (Elsevier, 2012).

Ji, J., K. Zhang, P. Clift, G. Zhuang, B. Song, X. Ke, and Y. Xu (2017), High-resolution magnetostratigraphic study of the Paleogene-Neogene strata in the Northern Qaidam Basin: Implications for the growth of the Northeastern Tibetan Plateau, Gondwana Research, 46, 141-155.

Kapp, P., J. D. Pelletier, A. Rohrmann, R. Heermance, J. Russell, and L. Ding (2011), Wind erosion in the Qaidam basin, central Asia: implications for tectonics,

paleoclimate, and the source of the Loess Plateau, GsA Today, 21(4/5), 4-10.
Kirschvink, J. (1980), The least-squares line and plane and the analysis of palaeomagnetic data, Geophysical Journal of the Royal Astronomical Society, 62(3), 699-718.
Li, J., L. Yue, A. Roberts, A. M. Hirt, F. Pan, L. Guo, Y. Xu, R. Xi, L. Guo, and X. Qiang (2018), Global cooling and enhanced Eocene Asian mid-latitude interior aridity, Nature communications, 9(1), 3026.
Li, Q., and X. Wang (2015), Discovery of Neogene beavers (Castoridae mammalia) in central Qaidam basin and their paleoenvironmental significance, Quaternary Science, 35(3), 12.
Licht, A., G. Dupont-Nivet, A. Pullen, P. Kapp, H. Abels, Z. Lai, Z. Guo, J. Abell, and D. Giesler (2016), Resilience of the Asian atmospheric circulation shown by Paleogene dust provenance, Nature communications, 7, 12390.
Liu, T. (1985), Loess and the Environment, China Ocean Press, Beijing.
Lowrie, W. (1990), Identification of ferromagnetic minerals in a rock by coercivity and unblocking temperature properties, Geophysical research letters, 17(2), 159-162.
Lu, H., X. Wang, and L. Li (2010), Aeolian sediment evidence that global cooling has driven late Cenozoic stepwise aridification in central Asia, Geological Society, London, Special Publications, 342(1), 29-44.
Lu, H., E. Wang, and K. Meng (2014), Paleomagnetism and anisotropy of magnetic susceptibility of the Tertiary Janggalsay section (southeast Tarim basin): Implications for Miocene tectonic evolution of the Altyn Tagh Range, Tectonophysics, 618, 67-78.
Lu, H., B. Fu, P. Shi, G. Xue, and H. Li (2018), Late-Miocene thrust fault-related folding in the northern Tibetan Plateau: Insight from paleomagnetic and structural analyses of the Kumkol basin, Journal of Asian Earth Sciences, 156, 246-255.
Ma, L., Y. Sun, R. Tada, Y. Yan, H. Chen, M. Lin, and K. Nagashima (2015), Provenance fluctuations of aeolian deposits on the Chinese Loess Plateau since the Miocene, Aeolian Research, 18, 1-9.

Malusà, M. G., and E. Garzanti (2019), The sedimentology of detrital thermochronology. In Fission-Track Thermochronology and its Application to Geology (pp. 123-143). Springer, Cham.

Malusà, M. G., and P. G. Fitzgerald (2020), The geologic interpretation of the detrital thermochronology record within a stratigraphic framework, with examples from the European Alps, Taiwan and the Himalayas, Earth-Science Reviews, 201, 103074.

McFadden, P., and M. McElhinny (1990), Classification of the reversal test in palaeomagnetism, Geophysical Journal International, 103(3), 725-729.

Molnar, P., W. R. Boos, and D. S. Battisti (2010), Orographic controls on climate and paleoclimate of Asia: thermal and mechanical roles for the Tibetan Plateau, Annual Review of Earth and Planetary Sciences, 38, 77-102.

Nie, J., A. Pullen, C. N. Garzione, W. Peng, and Z. Wang (2018), Pre-Quaternary decoupling between Asian aridification and high dust accumulation rates, Science advances, 4(2), eaao6977.

Nie, J., X. Ren, J. E. Saylor, Q. Su, and K. Pfaff (2020), Magnetic polarity stratigraphy, provenance, and paleoclimate analysis of Cenozoic strata in the Qaidam Basin, NE Tibetan Plateau, Geological Society of America Bulletin, 132(1-2), 310-320.

Nie, J., W. Peng, A. Möller, Y. Song, D. F. Stockli, T. Stevens, B. K. Horton, S. Liu, A. Bird, and J. Oalmann (2014), Provenance of the upper Miocene–Pliocene Red Clay deposits of the Chinese loess plateau, Earth and Planetary Science Letters, 407, 35-47.

Pang, J., J. Yu, D. Zheng, W. Wang, Y. Ma, Y. Wang, C. Li, Y. Li, and Y. Wang (2019), Neogene expansion of the Qilian Shan, north Tibet: Implications for the dynamic evolution of the Tibetan Plateau, Tectonics, 38, 1018-1032.

Pullen, A., P. Kapp, A. T. McCallister, H. Chang, G. E. Gehrels, C. N. Garzione, R. V. Heermance, and L. Ding (2011), Qaidam Basin and northern Tibetan Plateau as dust sources for the Chinese Loess Plateau and paleoclimatic implications, Geology, 39(11), 1031-1034.

Pye, K. (1987), Eolian Dust and Dust Deposits, Academic Press, London, p. 334.

Qiang, X., Z. Li, C. M. Powell, and H. Zheng (2001), Magnetostratigraphic record of the Late Miocene onset of the East Asian monsoon, and Pliocene uplift of northern Tibet, Earth and Planetary Science Letters, 187(1-2), 83-93.

Qiang, X., Z. An, Y. Song, H. Chang, Y. Sun, W. Liu, H. Ao, J. Dong, C. Fu, and F. Wu (2011), New eolian red clay sequence on the western Chinese Loess Plateau linked to onset of Asian desertification about 25 Ma ago, Science China Earth Sciences, 54(1), 136-144.

Ramstein, G., F. Fluteau, J. Besse, and S. Joussaume (1997), Effect of orogeny, plate motion and land–sea distribution on Eurasian climate change over the past 30 million years, Nature, 386(6627), 788.

Rea, D. K., H. Snoeckx, and L. H. Joseph (1998), Late Cenozoic eolian deposition in the North Pacific: Asian drying, Tibetan uplift, and cooling of the northern hemisphere, Paleoceanography, 13(3), 215-224.

Shen, X., S. Wan, C. France-Lanord, P. D. Clift, R. Tada, S. Révillon, X. Shi, D. Zhao, Y. Liu, and X. Yin (2017), History of Asian eolian input to the Sea of Japan since 15 Ma: Links to Tibetan uplift or global cooling?, Earth and Planetary Science Letters, 474, 296-308.

Song, Y., X. Fang, T. Masayuki, I. Naoto, J. Li, and Z. An (2001), Magnetostratigraphy of Late Tertiary sediments from the Chinese Loess Plateau and its paleoclimatic significance, Chinese Science Bulletin, 46(1), 16-21.

Sun, D., Z. An, J. Shaw, J. Bloemendal, and Y. Sun (1998), Magnetostratigraphy and palaeoclimatic significance of Late Tertiary aeolian sequences in the Chinese Loess Plateau, Geophysical Journal International, 134(1), 207-212.

Sun, J. (2002), Provenance of loess material and formation of loess deposits on the Chinese Loess Plateau, Earth and planetary science letters, 203(3-4), 845-859.

Sun, J., R. Zhu, and Z. An (2005), Tectonic uplift in the northern Tibetan Plateau since 13.7 Ma ago inferred from molasse deposits along the Altyn Tagh Fault, Earth and Planetary Science Letters, 235(3-4), 641-653.

Sun, Y., L. Ma, J. Bloemendal, S. Clemens, X. Qiang, and Z. An (2015), Miocene climate change on the Chinese Loess Plateau: Possible links to the growth of the northern Tibetan Plateau and global cooling, Geochemistry, Geophysics, Geosystems, 16(7), 2097-2108.

Tapponnier, P., Z. Xu, R. Françoise, M. Bertrand, A. Nicolas, W. Gérard, and J. Yang (2001), Oblique stepwise rise and growth of the Tibet plateau, Science, 294(5547), 1671-1677.

Vermeesch, P. (2009), RadialPlotter: A Java application for fission track, luminescence and other radial plots, Radiation Measurements, 44(4), 409-410.

Wan, S., A. Li, P. D. Clift, and J.-B. W. Stuut (2007), Development of the East Asian monsoon: mineralogical and sedimentologic records in the northern South China Sea since 20 Ma, Palaeogeography, Palaeoclimatology, Palaeoecology, 254(3-4), 561-582.

Wang, W., W. Zheng, P. Zhang, Q. Li, E. Kirby, D. Yuan, D. Zheng, C. Liu, Z. Wang, and H. Zhang (2017), Expansion of the Tibetan Plateau during the Neogene, Nature communications, 8, 15887.

Wei, Y., A. Xiao, L. Wu, L. Mao, H. Zhao, Y. Shen, and L. Wang (2016), Temporal and spatial patterns of Cenozoic deformation across the Qaidam Basin, Northern Tibetan Plateau, Terra Nova, 28(6), 409-418.

Yang, R., Y. Yang, X. Fang, X. Ruan, A. Galy, C. Ye, Q. Meng, and W. Han (2019), Late Miocene Intensified Tectonic Uplift and Climatic Aridification on the Northeastern Tibetan Plateau: Evidence From Clay Mineralogical and Geochemical Records in the Xining Basin, Geochemistry, Geophysics, Geosystems, 20(2), 829-851.

Yang, Y., A. Galy, X. Fang, R. Yang, W. Zhang, and J. Zan (2017), Eolian dust forcing of river chemistry on the northeastern Tibetan Plateau since 8 Ma, Earth and Planetary Science Letters, 464, 200-210.

Yin, A. (2010), Cenozoic tectonic evolution of Asia: A preliminary synthesis, Tectonophysics, 488(1-4), 293-325.

Zachos, J. C., G. R. Dickens, and R. E. Zeebe (2008), An early Cenozoic perspective on greenhouse warming and carbon-cycle dynamics, Nature, 451(7176), 279.

Zheng, D., P. Zhang, J. Wan, C. Li, and J. Cao (2003), Late Cenozoic deformation subsequence in northeastern margin of Tibet—Detrital AFT records from Linxia Basin, Science in China Series D: Earth Sciences, 46(2), 266-275.

Zhuang, G., J. K. Hourigan, B. D. Ritts, and M. L. Kent-Corson (2011), Cenozoic multiple-phase tectonic evolution of the northern Tibetan Plateau: Constraints from sedimentary records from Qaidam basin, Hexi Corridor, and Subei basin, northwest China, American Journal of Science, 311(2), 116-152.

Figure 1.

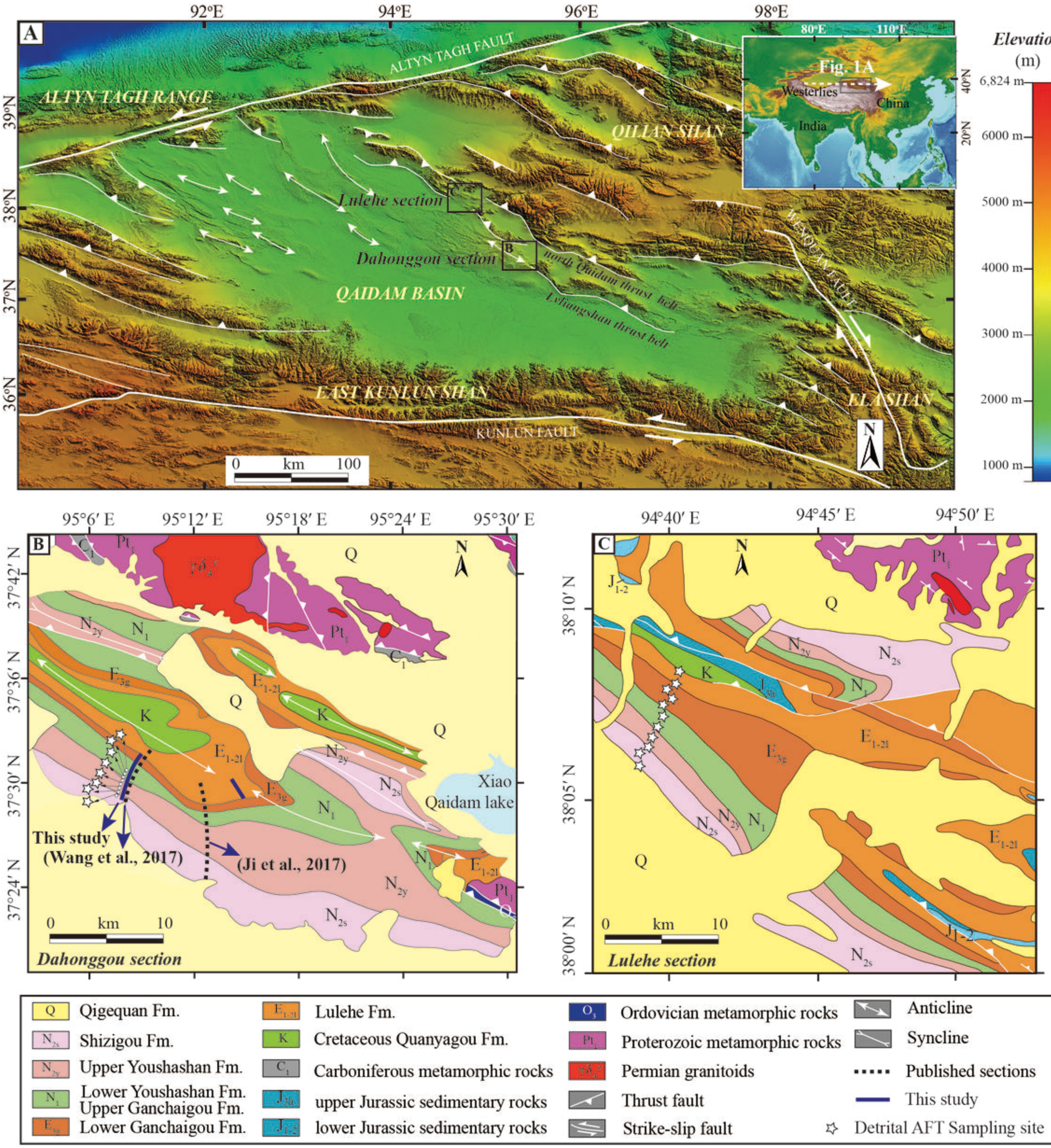

A
92ºE
94ºE
96ºE
98ºE
39ºN
38ºN
37ºN
36ºN
ALTYN TAGH FAULT
ALTYN TAGH RANGE
QILIAN SHAN
Lulehe section
Dahonggou section
north Qaidam thrust belt
Lvliangshan thrust belt
QAIDAM BASIN
WENQUAN FAULT
EAST KUNLUN SHAN
ELASHAN
KUNLUN FAULT
0 km 100
80ºE
110ºE
40ºN
20ºN
Fig. 1A
Westerlies
China
India
Elevation (m)
6,824 m
6000 m
5000 m
4000 m
3000 m
2000 m
1000 m
B
95°6′ E
95°12′ E
95°18′ E
95°24′ E
95°30′ E
37°42′ N
37°36′ N
37°30′ N
37°24′ N
Xiao Qaidam lake
This study
(Wang et al., 2017)
(Ji et al., 2017)
Dahonggou section
C
94°40′ E
94°45′ E
94°50′ E
38°10′ N
38°05′ N
38°00′ N
Lulehe section
Q Qigequan Fm.
N2s Shizigou Fm.
N2y Upper Youshashan Fm.
N1 Lower Youshashan Fm. Upper Ganchaigou Fm.
E3g Lower Ganchaigou Fm.
E1-21 Lulehe Fm.
K Cretaceous Quanyagou Fm.
C1 Carboniferous metamorphic rocks
J3h upper Jurassic sedimentary rocks
J1-2 lower Jurassic sedimentary rocks
O3 Ordovician metamorphic rocks
Pt1 Proterozoic metamorphic rocks
Permian granitoids
Thrust fault
Strike-slip fault
Anticline
Syncline
Published sections
This study
Detrital AFT Sampling site

Figure 2.

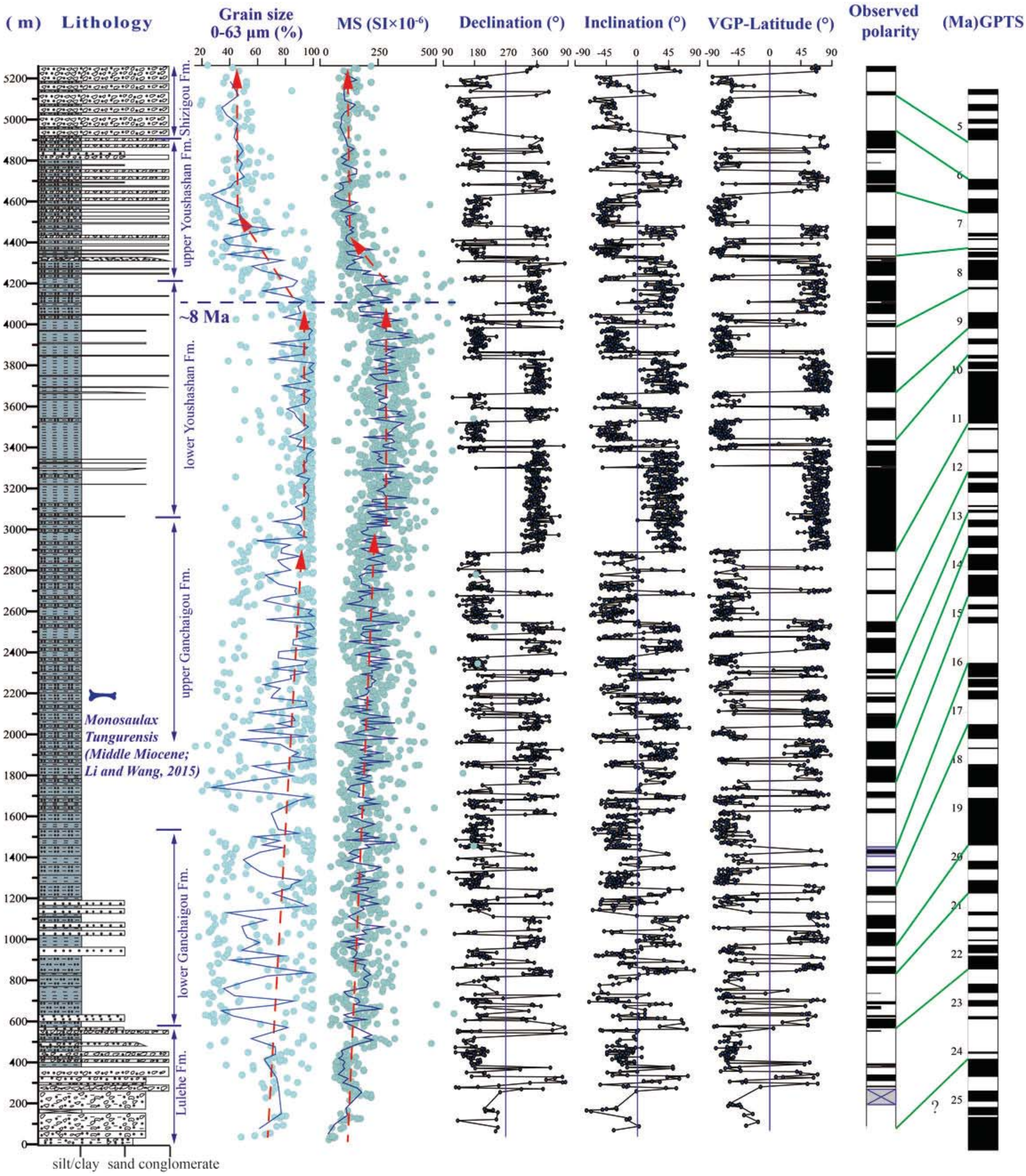
(m)
Lithology
Grain size 0-63 μm (%)
MS (SI×10-6)
Declination (°)
Inclination (°)
VGP-Latitude (°)
Observed polarity
(Ma)GPTS
Shizigou Fm.
upper Youshashan Fm.
lower Youshashan Fm.
upper Ganchaigou Fm.
lower Ganchaigou Fm.
Lulehe Fm.
~8 Ma
Monosaulax Tungurensis (Middle Miocene; Li and Wang, 2015)
silt/clay sand conglomerate

Figure 3.

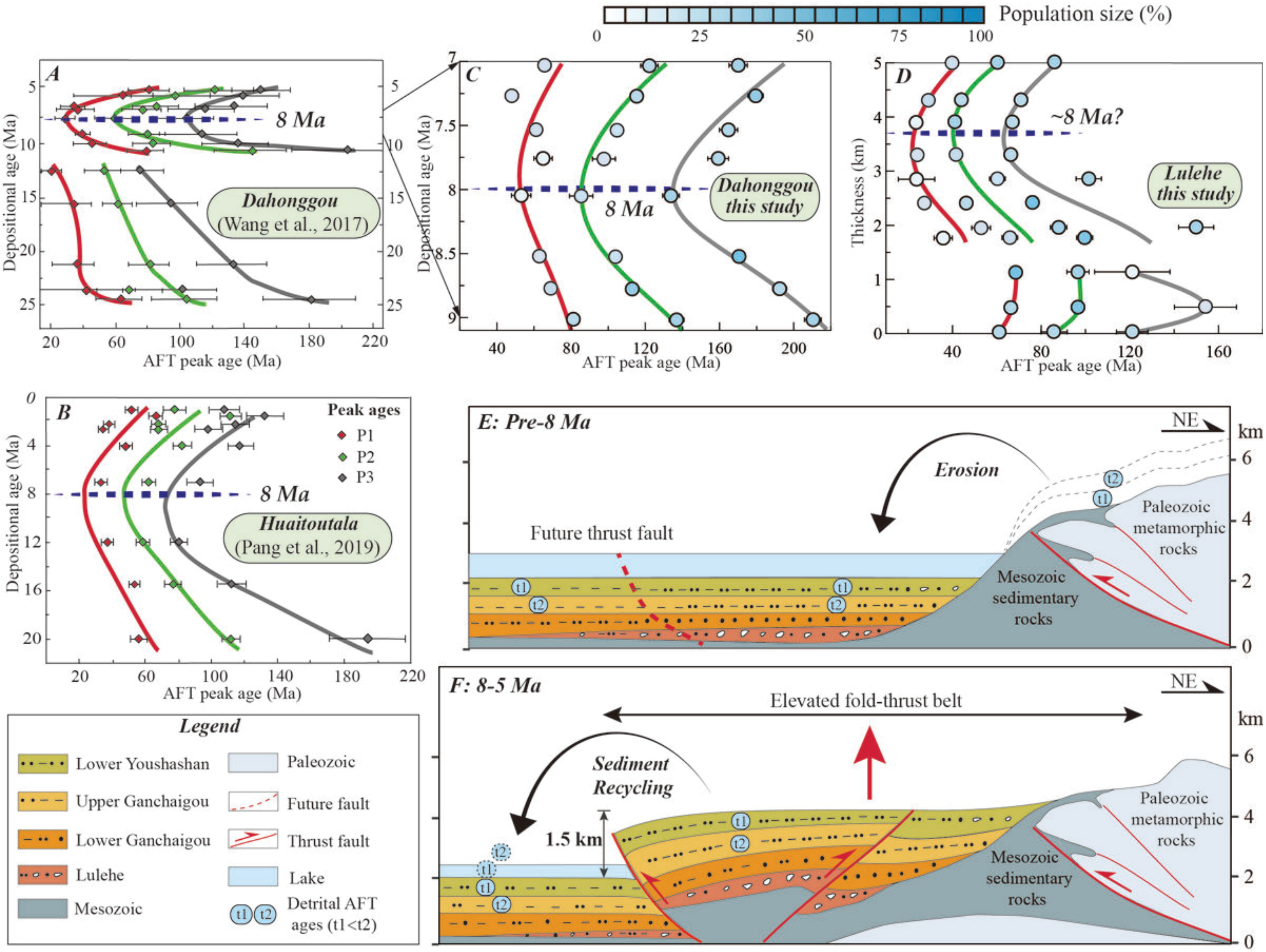

Population size (%)
0 25 50 75 100
A
8 Ma
Dahonggou
(Wang et al., 2017)
Depositional age (Ma)
AFT peak age (Ma)
C
8 Ma
Dahonggou this study
D
~8 Ma?
Lulehe this study
Thickness (km)
B
Peak ages
P1
P2
P3
Huaitoutala
(Pang et al., 2019)
E: Pre-8 Ma
NE
km
Erosion
Future thrust fault
Paleozoic metamorphic rocks
Mesozoic sedimentary rocks
F: 8-5 Ma
Elevated fold-thrust belt
Sediment Recycling
1.5 km
Legend
Lower Youshashan
Upper Ganchaigou
Lower Ganchaigou
Lulehe
Mesozoic
Paleozoic
Future fault
Thrust fault
Lake
Detrital AFT ages (t1<t2)

Figure 4.

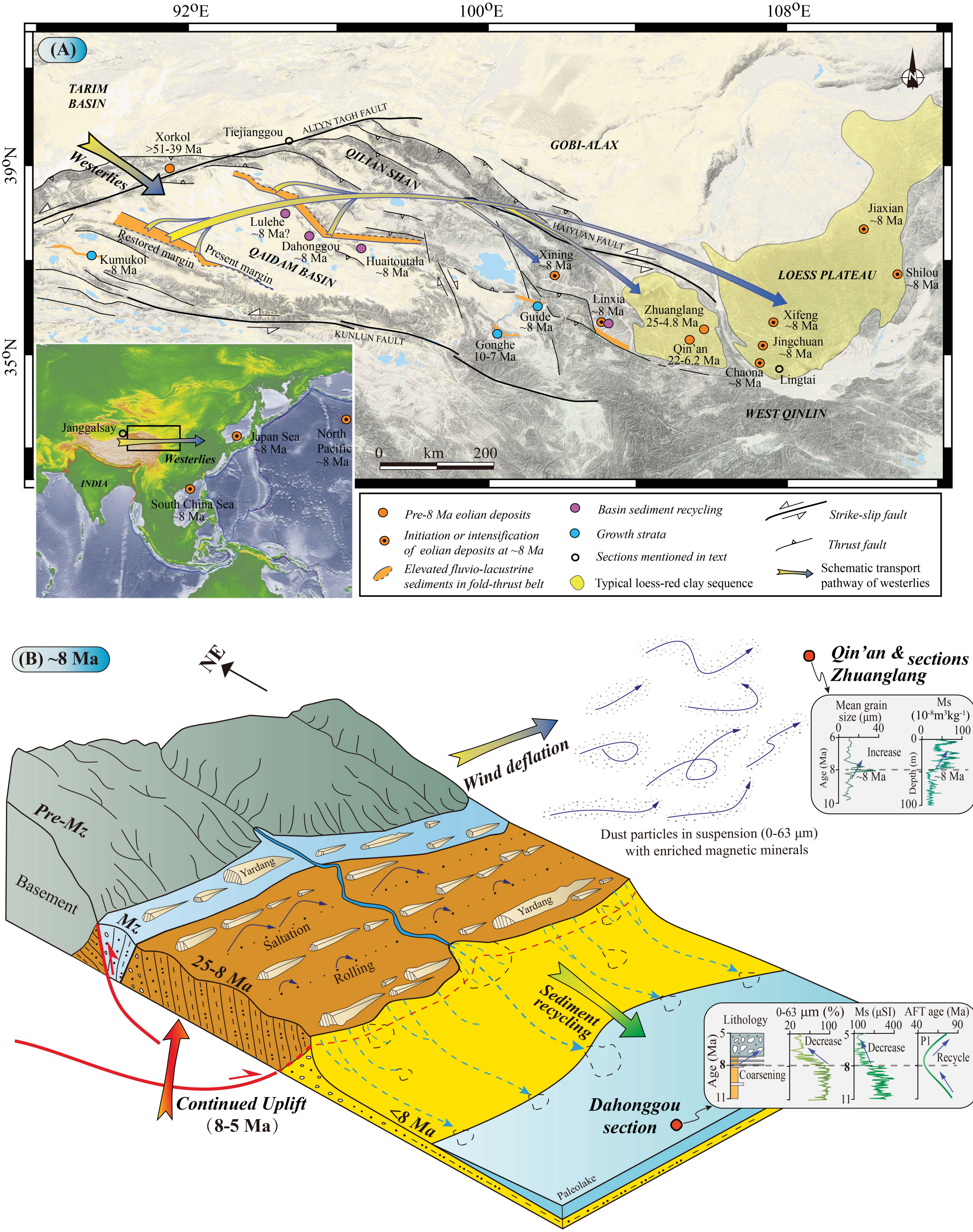

92°E
100°E
108°E
39°N
35°N
(A)
TARIM BASIN
Westerlies
Xorkol
>51-39 Ma
Tiejianggou
ALTYN TAGH FAULT
QILIAN SHAN
GOBI-ALAX
Lulehe
~8 Ma?
Dahonggou
~8 Ma
Huaitoutala
~8 Ma
Restored margin
Present margin
QAIDAM BASIN
Kumukol
~8 Ma
HAIYUAN FAULT
Xining
~8 Ma
Guide
~8 Ma
Linxia
~8 Ma
Gonghe
10-7 Ma
KUNLUN FAULT
Zhuanglang
25-4.8 Ma
Qin'an
22-6.2 Ma
Jiaxian
~8 Ma
Shilou
~8 Ma
LOESS PLATEAU
Xifeng
~8 Ma
Jingchuan
~8 Ma
Chaona
~8 Ma
Lingtai
WEST QINLIN
0 km 200
Janggalsay
Japan Sea
~8 Ma
North
Pacific
~8 Ma
Westerlies
INDIA
South China Sea
~8 Ma
Pre-8 Ma eolian deposits
Initiation or intensification of eolian deposits at ~8 Ma
Elevated fluvio-lacustrine sediments in fold-thrust belt
Basin sediment recycling
Growth strata
Sections mentioned in text
Typical loess-red clay sequence
Strike-slip fault
Thrust fault
Schematic transport pathway of westerlies
(B) ~8 Ma
NE
Wind deflation
Dust particles in suspension (0-63 μm)
with enriched magnetic minerals
Qin'an & Zhuanglang sections
Mean grain size (μm)
Ms ($10^{-8}m^3kg^{-1}$)
Increase
~8 Ma
Age (Ma)
Depth (m)
Pre-Mz
Basement
Mz
Yardang
Saltation
Rolling
25-8 Ma
Sediment recycling
Continued Uplift
(8-5 Ma)
<8 Ma
Dahonggou section
Paleolake
Lithology
0-63 μm (%)
Ms (μSI)
AFT age (Ma)
Decrease
Coarsening
P1
Recycle

Figure 5.

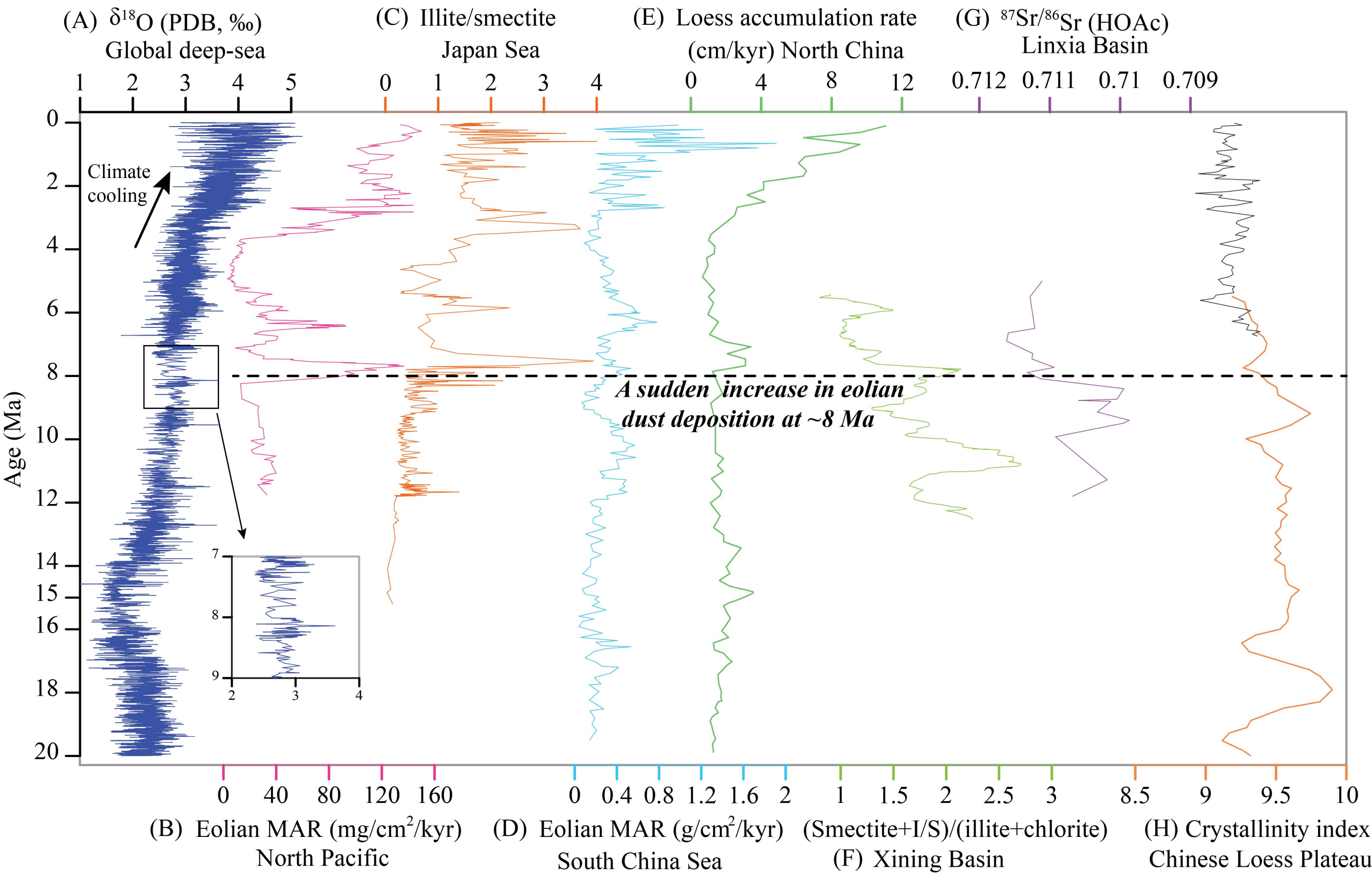

(A) δ18O (PDB, ‰)
Global deep-sea
(C) Illite/smectite
Japan Sea
(E) Loess accumulation rate
(cm/kyr) North China
(G) 87Sr/86Sr (HOAc)
Linxia Basin
Age (Ma)
Climate
cooling
A sudden increase in eolian
dust deposition at ~8 Ma
(B) Eolian MAR (mg/cm2/kyr)
North Pacific
(D) Eolian MAR (g/cm2/kyr)
South China Sea
(Smectite+I/S)/(illite+chlorite)
(F) Xining Basin
(H) Crystallinity index
Chinese Loess Plateau